

AperTO - Archivio Istituzionale Open Access dell'Università di Torino

**Quantification of iopamidol multi-site chemical exchange properties for ratiometric chemical exchange saturation transfer (CEST) imaging of pH**

**This is the author's manuscript**

*Original Citation:*

*Availability:*

This version is available <http://hdl.handle.net/2318/1656381> since 2018-01-12T13:35:03Z

*Published version:*

DOI:10.1088/0031-9155/59/16/4493

*Terms of use:*

Open Access

Anyone can freely access the full text of works made available as "Open Access". Works made available under a Creative Commons license can be used according to the terms and conditions of said license. Use of all other works requires consent of the right holder (author or publisher) if not exempted from copyright protection by the applicable law.

(Article begins on next page)

# Quantification of iopamidol multi-site chemical exchange properties for ratiometric chemical exchange saturation transfer (CEST) imaging of pH

Phillip Zhe Sun <sup>1\*</sup>, Dario Livio Longo <sup>2</sup>, Wei Hu <sup>3</sup>, Gang Xiao <sup>3,4</sup>, and Renhua Wu <sup>3\*</sup>

<sup>1</sup> Athinoula A. Martinos Center for Biomedical Imaging, Department of Radiology, Massachusetts General Hospital and Harvard Medical School, Charlestown, MA, USA

<sup>2</sup> Institute for Biostructures and Bioimages (CNR) c/o Molecular Biotechnology Center and Molecular Imaging Center, University of Torino, Italy

<sup>3</sup> Department of Radiology, 2<sup>nd</sup> Affiliated Hospital of Shantou University Medical College, China

<sup>4</sup> Department of Math and Applied Mathematics, Hanshan Normal University, Chaozhou, China

\* Corresponding author:

Dr. Phillip Zhe Sun ([pzhesun@nmr.mgh.harvard.edu](mailto:pzhesun@nmr.mgh.harvard.edu))

Athinoula A. Martinos Center for Biomedical Imaging

Department of Radiology, MGH and Harvard Medical School

Rm 2301, 149 13<sup>th</sup> Street, Charlestown, MA 02129

Phone: 617-726-4060, Fax: 617-726-7422

Or Dr. Renhua Wu ([rhwu@stu.edu.cn](mailto:rhwu@stu.edu.cn))

2<sup>nd</sup> Affiliated Hospital of Shantou University Medical College

Shantou 515041, Guangdong, China

Tel: (86) 0754-88915674

**Running Head:** Quantification of iopamidol CEST properties for imaging pH

**Word Count:** 3,068

**ACKNOWLEDGEMENTS** This study was supported in part by grants from NIH/NIBIB 1K01EB009771, NIH/NINDS 1R01NS083654, Regione Piemonte (NanoIGT-CIPE2007) and NSFC 30930027. The authors would like to thank Dr. Chongzhao Ran for helpful discussions and Bracco Imaging, S.p.A., Milan, Italy for generously providing iopamidol samples.

## ABSTRACT

pH-sensitive chemical exchange saturation transfer (CEST) MRI holds great promise for in vivo applications. However, CEST effect depends on not only exchange rate and hence pH, but also on the contrast agent concentration, which must be determined independently in order to quantify pH. Ratiometric CEST MRI normalizes the concentration effect by comparing CEST measurements of multiple labile protons from the same molecule to simplify pH determination. Iopamidol, a commonly used X-Ray contrast agent, has been explored as a ratiometric CEST agent for imaging pH. However, iopamidol CEST properties have not been solved, determination of which is important for optimization and quantification of iopamidol pH imaging. Our study applied Bloch-McConnell equations and numerically solved iopamidol multi-site pH-dependent chemical exchange properties. We found that iopamidol CEST MRI is suitable for measuring pH between 6 and 7.5 with an accuracy of 0.1 pH unit despite that  $T_1$  and  $T_2$  measurements varied substantially with pH and concentration. Moreover, we determined base-catalyzed chemical exchange for both 2-hydroxypropanamido ( $k_{sw}=1.2 \times 10^{pH-4.1}$ ) and amide ( $k_{sw}=1.2 \times 10^{pH-4.6}$ ) proton groups that are statistically different from each other ( $P < 0.01$ , ANCOVA), understanding of which should help guide optimization and translation of iopamidol pH imaging under various experimental conditions.

**Keywords:** chemical exchange saturation transfer (CEST); iopamidol; MRI; pH

## 1. INTRODUCTION

Chemical exchange saturation transfer (CEST) MRI is sensitive to microenvironment properties including pH, temperature, metabolites, metal ions, and enzyme activities, and has been increasingly applied in vivo (Ward *et al.*, 2000; Aime *et al.*, 2002; Zhang *et al.*, 2005; Sun and Sorensen, 2008; Woods *et al.*, 2006; van Zijl and Yadav, 2011; Olatunde *et al.*, 2012; Dula *et al.*, 2012; Hingorani *et al.*, 2013; Vinogradov *et al.*, 2013; Castelli *et al.*, 2013). Particularly, CEST MRI is sensitive to pH, an informative biomarker for metabolic disruption in disorders such as acute ischemic stroke and renal injury (Jokivarsi *et al.*, 2007; Sun *et al.*, 2007b; Sun *et al.*, 2011a; Chan *et al.*, 2013; Jin *et al.*, 2012; Sun *et al.*, 2012). However, CEST MRI contrast varies not only with exchange rate, and hence pH, but also with the CEST agent concentration, bulk water relaxation rates and experimental conditions (Sun *et al.*, 2005; Terreno *et al.*, 2010; Wu *et al.*, 2012; Sun, 2012; Zaiss and Bachert, 2013; Sun *et al.*, 2014a). Because the labile proton concentration has to be independently determined in order to derive pH, the conventional CEST imaging only provides pH-weighted information (Sun, 2010b; Zu *et al.*, 2012; Sun *et al.*, 2013b). To address this limitation, ratiometric CEST MRI has been proposed that normalizes the confounding concentration effect for simplifying pH measurement (Ward and Balaban, 2000; Ali *et al.*, 2009; Liu *et al.*, 2012). A particularly interesting ratiometric MRI agent is iopamidol, approved by food and drug administration (FDA) as a X-Ray contrast agent since 1980s, which has been recently shown capable of imaging renal pH (Longo *et al.*, 2012; Longo *et al.*, 2011; Aime *et al.*, 2005).

Because of the tremendous interest in investigating iodinated agents for pH imaging, it is important to quantify their CEST properties, which should shed light on their sensitivity and detectability. Briefly, we used the Bloch-McConnell equations to describe multi-site iopamidol CEST effects (Woessner *et al.*, 2005; McMahon *et al.*, 2006; Sun *et al.*, 2007a; Li *et al.*, 2008; Murase and Tanki, 2011; Sun, 2010a). We numerically derived multi-site labile proton ratio and exchange rate, and found that chemical exchange for both 2-hydroxypropanamido and amide protons are dominantly base-catalyzed for the range of pH we investigated. We also determined the accuracy of iopamidol pH imaging is 0.1 pH unit despite that  $T_1$  and  $T_2$  measurements varied substantially with pH and concentration. Because

understanding of iopamidol exchange properties is necessary for optimizing the pulsed-RF irradiation in clinic, our study should aid clinical translation of iopamidol pH imaging (Sun *et al.*, 2008; Sun *et al.*, 2011b; Schmitt *et al.*, 2011; Sun *et al.*, 2013a; Zhu *et al.*, 2010; Zu *et al.*, 2011).

## 2. MATERIALS AND METHODS

### Phantom

We prepared 20 and 40 mM iopamidol (Bracco Imaging, S.p.A., Milan, Italy) phosphate buffered solution with pH titrated to 5.5, 6, 6.5, 7, 7.5 and 8 (EuTech pH Meter, Singapore). The solution was transferred into micro-centrifuge tubes and then inserted into two separate phantom containers. The phantom containers were filled with low gelling point agarose solution and solidified under room temperature.

### MRI and Data Processing

Experiments were obtained using a 4.7 Tesla MRI scanner (Bruker Biospec, Billerica, MA) at room temperature. Image readout was single-shot echo planner imaging (EPI) with a field of view of 48x48 mm, image matrix =64x64 and slice thickness =3 mm.  $T_1$  was measured using inversion recovery MRI, with seven inversion times (TI) ranging from 100 to 7,500 ms. We chose a long recovery time between image readout and the next inversion pulse to be 12,000 ms so that steady state could be obtained. The echo time (TE) was 39.5 ms and number of average (NSA) was 2. For  $T_2$  MRI, we used SE EPI with six TE from 50 to 1,000 ms (TR=12,000 ms, NSA =2). For CEST MRI, we obtained Z-spectra ranging from -7 to 7 ppm, at intervals of 0.25 ppm (i.e.,  $\pm 1400$  Hz per 50 Hz at 4.7T). Continuous wave (CW) RF saturation was applied for 5 s (TS), with its amplitude varied from 1, 1.5, 2, 2.5, 3 to 4  $\mu$ T (TR/TE =12,000/39.5 ms, NSA =2).

Data were processed in MATLAB (MathWorks, Natick, MA).  $T_1$  and  $T_2$  were obtained by least squares fitting of the image intensity as a function of inversion time and echo time, respectively. We fit asymmetry plots using modified Bloch-McConnell equations (Sun, 2010a). CEST effect was calculated using CEST ratio (CESTR)

$$\text{CESTR} = \frac{I_{\text{ref}} - I_{\text{label}}}{I_0} \quad (1)$$

where  $I_{\text{ref}}$  and  $I_{\text{label}}$  are the reference and label scans, and  $I_0$  is the control scan (i.e.,  $B_1 = 0$ ). pH sensitive ratiometric CEST effect was calculated using relative CESTR and inverse relative saturation transfer ( $\text{RST}_{\text{inv}}$ ), as defined by Longo et al (Longo *et al.*, 2011). Specifically, we have

$$\text{rCESTR} = \text{CESTR}_{4.3\text{ppm}} / \text{CESTR}_{5.5\text{ppm}} \quad (2)$$

$$\begin{aligned} \text{RST}_{\text{inv}} &= \frac{\text{CESTR}_{4.3\text{ppm}}}{\text{CESTR}_{5.5\text{ppm}}} \cdot \left( \frac{1 - \text{CESTR}_{5.5\text{ppm}}}{1 - \text{CESTR}_{4.3\text{ppm}}} \right) \\ &= \text{rCESTR} \cdot (1 + \eta) \end{aligned} \quad (3)$$

where  $\eta = \frac{\text{CESTR}_{4.3\text{ppm}} - \text{CESTR}_{5.5\text{ppm}}}{1 - \text{CESTR}_{4.3\text{ppm}}}$ . In addition, the contrast to noise ratio (CNR) between pH 6 and

7.5 was calculated using (Sun *et al.*, 2013a)

$$\text{CNR} = \frac{\text{CESTR}|_{\text{pH}=7.5} - \text{CESTR}|_{\text{pH}=6}}{\sqrt{(\sigma_{\text{pH}=7.5}^2 + \sigma_{\text{pH}=6}^2)/2}} \quad (4)$$

where CESTR and  $\sigma$  represent the mean CESTR and its standard deviation for each pH compartment. For the numerical fitting, we fixed the relative labile proton ratio for 5.5 (2-hydroxypropanamido group), 4.3 (amide group), 1.8 (secondary hydroxyl group) and 0.8 (primary hydroxyl groups) ppm be 1:2:1:4. Eleven parameters were determined from the numerical fitting, including  $T_{1w}$ ,  $T_{2w}$ , 2-hydroxypropanamido labile proton ratio, and labile proton exchange rate and  $T_{2s}$  for each labile proton at 5.5, 4.3, 1.8 and 0.8 ppm. We used least squares optimization to minimize the error function, given

as  $\epsilon = \sum_{\delta=0.75}^{7\text{ppm}} (\text{CESTR}_{\text{fit}}(\delta) - \text{CESTR}_{\text{exp}}(\delta))^2$ . The fitting was repeated for each pH and RF power level. Results

were reported as mean  $\pm$  standard deviation and P values less than 0.05 were considered statistically significant.

### 3. RESULTS

Fig. 1 compares simulated Z-spectra and asymmetry plots of two exchangeable sites at 4.3 and 5.5 ppm with their labile proton ratio with respect to bulk water being 1:1500 and 1:3000 at exchange rates of 50 and 200 s<sup>-1</sup>, respectively (B<sub>1</sub> = 2.5 μT, TS = 5 s). We chose representative relaxation rates of T<sub>1w</sub> = 3 s, T<sub>1s</sub> = 1 s, T<sub>2s</sub> = 0.5 s, and varied T<sub>2w</sub> from 1 to 2 s. CEST effects could be observed at 4.3 and 5.5 ppm (Fig. 1a). Z-spectral signal close to the bulk water resonance strongly depends on T<sub>2w</sub> due to direct RF saturation. Because the asymmetry analysis subtracts the symmetric direct RF saturation effect, it is substantially less susceptible to T<sub>2w</sub> variation. We measured the change in Z-spectra and asymmetry plots from those simulated assuming the median T<sub>2w</sub> (i.e., 1.5 s). Fig. 1b shows that the normalized sum of squares (i.e.,  $\sum_{i=1}^N \left( I_{i,T_{2w}} - I_{i,\overline{T_{2w}}} \right)^2 / N$ ) is significantly higher in Z-spectrum than asymmetry plot (2.85 ± 3.06 vs. 0.01 ± 0.01, P < 0.01). Because the asymmetry plot is less susceptible to moderate T<sub>2w</sub> difference than Z-spectra, we chose to solve iopamidol CEST properties by fitting the asymmetry plots.

Fig. 2 evaluates pH-sensitive iopamidol CEST imaging. Fig. 2a shows three representative Z-spectra at pH of 6, 7 and 8 (B<sub>1</sub> = 2.5 μT). It is important to note that CEST effects from amide (4.3 ppm) and 2-hydroxypropanamido (5.5 ppm) could be reasonably resolved for pH 6 and 7, they however, merged into one broad peak at pH of 8. Fig. 2b shows CEST asymmetry ratio (CESTR) calculated at 4.3 (circles) and 5.5 ppm (squares). While CEST effect initially increased with pH, CESTR at 5.5 ppm peaked at pH of 7 and CESTR at 4.3 ppm peaked at pH of 7.5 (Fig. 2b). The unequal pH dependence of CESTR at 4.3 and 5.5 ppm enables ratiometric pH quantification. Fig. 2c shows that the rCESTR increases from 0.6 ± 0.1 to 2.3 ± 0.1 for pH at 6 and 7.5, respectively. We also measured T<sub>1</sub> and T<sub>2</sub>. T<sub>1</sub> decreased substantially with concentration (P < 0.01, 2-sample t-test) but showed little pH dependence (P > 0.15, linear regression). T<sub>1w</sub> was 2.68 ± 0.01 s and 2.51 ± 0.01 s for 20 and 40 mM iopamidol solutions, respectively. In contrast, T<sub>2</sub> decreased substantially with pH (P < 0.01, linear regression) and concentration (P < 0.01, paired t-test). For 20 mM iopamidol solution, T<sub>2w</sub> (pH) = 2.46 - 0.23 \* pH (s), whereas for 40 mM, T<sub>2w</sub> (pH) = 1.93 - 0.20 \* pH (s).

We investigated the optimal RF irradiation level for ratiometric pH imaging. Fig. 3a shows measured CESTR at 4.3 (circles) and 5.5 ppm (squares) for pH of 6 and 7.5 ( $B_1=2.5 \mu\text{T}$ ). CESTR increased with RF irradiation level, suggesting that a relatively high  $B_1$  irradiation field is needed to efficiently saturate iopamidol labile groups. Whereas CESTR at 5.5 ppm was higher than that at 4.3 ppm for pH of 6, the relative magnitude of CEST effect at 5.5 and 4.3 ppm reversed at pH of 7.5. We quantified ratiometric pH MRI using two indices: rCESTR and  $\text{RST}_{\text{inv}}$ , as defined by Longo et al (Longo *et al.*, 2011). The contrast to noise ratio (CNR) between pH 6 and 7.5 compartments initially increased with  $B_1$  and peaked at an intermediate  $B_1$  of  $2.5 \mu\text{T}$  (Fig. 3b). This shows that whereas the magnitude of pH contrast measured by  $\Delta\text{RST}_{\text{inv}}$  is statistically higher than that of  $\Delta\text{rCESTR}$  ( $P<0.01$ , ANCOVA), there was relatively small difference in CNR up to the optimal  $B_1$  saturation field. Fig. 3c shows the ratiometric CESTR map, demonstrating good pH contrast between 6 and 7.5.

We determined the accuracy of iopamidol pH mapping. Fig. 4a shows that the logarithmic rCESTR can be described by polynomial regression ( $\log_{10}(\text{rCESTR})=0.13\text{pH}^2-1.34\text{pH}+3.26$ ) for 40 mM iopamidol solution, with  $R^2=0.998$  ( $P<0.01$ ). The polynomial regression enables derivation of absolute pH map from pH-weighted rCESTR image for 40 mM (Fig. 4b) and 20 mM iopamidol (Fig. 4c). For 40 mM iopamidol, we found being  $5.99\pm0.23$ ,  $6.46\pm0.06$ ,  $7.03\pm0.02$  and  $7.49\pm0.02$  for pH of 6.0, 6.5, 7.0 and 7.5, respectively. pH determined from MRI strongly correlates with calibrated pH,  $\text{pH}(\text{MRI})=1.01\text{pH}-0.10$  ( $P<0.01$ ). Moreover, the intercept is not significant different from zero, suggesting no systematic biases in pH determination. For 20 mM iopamidol, we found being  $6.01\pm0.36$ ,  $6.46\pm0.20$ ,  $7.09\pm0.08$  and  $7.55\pm0.08$  for pH of 6.0, 6.5, 7.0 and 7.5, respectively. We found pixel-wise determined pH for 20 mM iopamidol is  $\text{pH}(\text{MRI})=1.03\text{pH}-0.15$  ( $P<0.01$ ). The intercept is not statistically significant different from zero (Fig. 4d). Our data showed that the standard deviation was higher at lower pH and iopamidol concentration, suggesting that it is governed by signal to noise ratio (SNR) of CEST MRI measurement. This is because exchange rate is reduced at lower pH, hence the CEST effect and SNR decreases with pH and iopamidol concentration. Because sensitivity can be improved with signal averaging, use of sensitive hardware and novel pulse sequence designs (Sun *et al.*, 2014b), the pH accuracy for the ratiometric iopamidol MRI approach can be reasonably determined using the maximal difference between the measurement mean



and the theoretical value, within  $\pm 0.1$ . Both  $\chi^2$  and  $R^2$  tests showed good fitting. We found  $\chi^2$  was less than  $10^{-3}$  for pH measurement from both iopamidol solutions, substantially smaller than  $\chi^2_{0.05}$  (i.e., 7.82) for three degrees of freedom. In addition,  $R^2$  was higher than 0.99 for pH measurement from both iopamidol solutions. Furthermore, ANCOVA analysis of pH measurements from 20 and 40 mM iopamidol phantoms showed no significant effect of iopamidol concentration on pH calibration, confirming that iopamidol ratiometric pH imaging can indeed measure pH despite a substantial difference in iopamidol concentration.

We numerically solved iopamidol CEST properties using the Bloch-McConnell equations. Because CEST peaks could not be resolved at pH of 8 due to very fast chemical exchange, we numerically fit CEST asymmetry plots for pH from 5.5 to 7.5 under  $B_1$  irradiation level of 1, 1.5, 2, 2.5, 3 and 4  $\mu$ T. Due to non-negligible CEST effects from hydroxyl groups, a five-pool exchange model was chosen to describe iopamidol CEST measurements, including 2-hydroxypropanamido protons (5.5 ppm), amide (4.3 ppm), two chemically not-equivalent hydroxyl groups (1.8 and 0.8 ppm) and bulk water (set to be 0 ppm). In addition, we set labile proton  $T_1$  ( $T_{1s}$ ) to be 1 s due to the use of long RF irradiation.  $B_0$  inhomogeneity was determined to be  $5 \pm 6$  Hz. Nevertheless, to reduce field inhomogeneity effect very close to bulk water signal, we fit CEST asymmetry from 0.75 to 7 ppm. The numerical fitting and experimental data under the optimal RF power level of 2.5  $\mu$ T were shown in Fig. 5a. The coefficient of determination ( $R^2$ ) for all pH values was  $0.99 \pm 0.01$ , and the squared residuals error between numerical fitting and experimental measurements was  $0.30 \pm 0.77\%$ . The fitting took approximately 4 min for each RF power level. Fig. 5b shows that the exchange rate at 4.3 and 5.5 ppm can be reasonably described using a dominantly base-catalyzed exchange equation (i.e.,  $k_{sw} = k_0 + k_b \cdot 10^{\text{pH} - \text{pK}_w}$ ). We found  $k_{sw}(5.5 \text{ ppm}) = 1.2 \cdot 10^{\text{pH} - 4.1}$  for 2-hydroxypropanamido protons and  $k_{sw}(4.3 \text{ ppm}) = 1.2 \cdot 10^{\text{pH} - 4.6}$  for amide protons (Table 1). Statistical test of logarithmic exchange rate confirmed significant difference in their exchange rate ( $P < 0.01$ , ANCOVA). In addition, the 2-hydroxypropanamido labile proton ratio with respect to bulk water can be estimated to be 1:2778, while that solved from numerical fitting was  $1:3449 \pm 747$ , not significantly different from the theoretical estimation ( $P > 0.05$ , one sample t-test). Moreover, numerical fitting determined  $T_{1w} = 3.5 \pm 0.3$  s,  $T_{2w} = 1.6 \pm 0.1$  s, and  $T_{2s}$  was  $0.6 \pm 0.3$ ,  $1.5 \pm 0.4$ ,  $0.7 \pm 0.4$  and  $0.8 \pm 0.2$  s for 2-hydroxypropanamido protons

(5.5 ppm), amide (4.3 ppm), and two hydroxyl groups at (1.8 and 0.8 ppm), respectively. Understanding pH-dependent exchange properties should help guide experimental optimization and quantification of iopamidol pH imaging under various experimental conditions such as pulsed RF irradiation scheme at different field strength.

#### 4. DISCUSSION

Our study quantitatively solved the multi-site exchange properties of iopamidol. We confirmed that iopamidol ratiometric CEST MRI is capable of measuring pH from 6 to 7.5 at 4.7 T with an accuracy of 0.1 pH unit despite that  $T_1$  and  $T_2$  measurements varied substantially with pH and concentration. Iopamidol pH imaging is promising to complement pH measurement techniques including pH-weighted CEST MRI,  $^{31}\text{P}$  MR spectroscopy (MRS), and dual modality (positron emission tomography (PET)-MRI) contrast-enhanced imaging (Adam *et al.*, 1986; Frullano *et al.*, ; Sheth *et al.*, 2012). Clinical iopamidol dosage is procedure specific. For example, the recommended dosage is 40-150 ml of Isovue 300-370 for whole body computer tomography enhancement (Iopamidol Product Monograph). In this case, the iopamidol concentration in blood can be estimated to be about 6-29 mM. Iopamidol concentration is also organ specific, likely being more concentrated in kidney and bladder. Indeed, Longo *et al.* have successfully imaged acute renal injury-induced pH change using iopamidol ratiometric CEST MRI (Longo *et al.*, 2012). Accurate pH imaging can complement a number of MRI applications (Kogan *et al.*, 2014; Dagher *et al.*, 2000). For example, Dagher *et al.* showed that urea, an important kidney metabolite, can be imaged using CEST MRI (Dagher *et al.*, 2000). Because urea hydroxyl chemical exchange is pH-dependent, pH has to be measured independently in order to derive urea concentration, for which iopamidol pH MRI is applicable.

Because high magnetic field provides enhanced sensitivity for diamagnetic CEST (DIACEST) MRI, iodinated contrast agent-based pH imaging has been initially demonstrated at 7 Tesla (Chen *et al.*, 2013; Longo *et al.*, 2012). In addition to more efficient spin polarization,  $T_1$  also increases at high field strength,

leading to stronger CEST effect. Moreover, because the frequency shift in Hz scales linearly with field strength, the concomitant direct RF saturation is reduced at high field. We here demonstrated iopamidol pH imaging at 4.7 Tesla, substantiating its translation potential. We also compared two means of pH calculation: rCESTR and  $RST_{inv}$ . Whereas  $\Delta RST_{inv}$  is statistically larger than  $\Delta rCESTR$  between pH 6 and 7.5, there was relatively small difference in their CNR due to error propagation from the correction factor (Fig. 3). It is important to note that because our ability to resolve pH difference relies upon CNR, both rCESTR and  $RST_{inv}$  provide similar pH sensitivity. Our study showed that pH can be accurately determined despite substantial pH and iopamidol concentration-induced  $T_1$  and  $T_2$  change. Also, worth noting is that iopamidol labile proton groups are reasonably close to endogenous amide protons and semisolid macromolecules, which may have to be considered in order to quantify in vivo ratiometric pH imaging (Henkelman *et al.*, 1994; Zhou *et al.*, 2004; Jones *et al.*, 2013; Scheidegger *et al.*, 2011). It has been shown by Chen *et al.* that Lorentzian line shape fitting could overcome the NOE and MT contributions and enable extracellular pH determination within in vivo tumors (Chen *et al.*, 2013).

It is necessary to note that it is technically challenging to determine exchange properties in a multi-site CEST system.  $T_2$ -based solution could not resolve multi-site exchange (Aime *et al.*, 2005). Although the Lorentzian spectral analysis is capable of estimating exchange rate, it is difficult to solve multi-site exchange that are close to each other (Allerhand *et al.*, 1966). Our work addressed an important aspect of quantitative CEST analysis. We showed that the modified Bloch-McConnell equations can reasonably describe multi-site CEST phenomenon, with small residual errors between the fitting and experimental measurement. The numerically solved labile proton ratio is in reasonable agreement with estimation, and the exchange rate can be well described by a base-catalyzed chemical exchange relationship. While it is necessary to include hydroxyl groups in order to fit the asymmetry plots at 4.3 and 5.5 ppm, hydroxyl chemical exchange rates are in the fast exchange regime. Therefore, the numerically derived exchange rates for hydroxyl groups may be subject to non-negligible fitting errors but provide good estimates of their order of magnitude. It is important to note that understanding pH-dependent exchange properties could help guide experimental optimization and quantification of iopamidol pH imaging. Briefly, because continuous wave (CW) RF irradiation scheme is not routinely

available on clinical scanners, pulsed RF irradiation has to be chosen. The irradiation pulse duration, flip angle and inter-pulse delay of CEST MRI have to be optimized based on chemical exchange rate and pulse sequence (Sun *et al.*, 2008; Sun *et al.*, 2011b; Schmitt *et al.*, 2011; Sun *et al.*, 2013a; Zhu *et al.*, 2010; Sun *et al.*, 2014b). Therefore, determination of pH-dependent exchange rate should aid clinical translation of iopamidol pH imaging.

## 5. CONCLUSION

Our study numerically derived multi-site iopamidol exchange properties and showed that chemical exchange rates for 2-hydroxypropanamido and amide groups were dominantly base-catalyzed and statistically different from each other, making iopamidol a sensitive ratiometric pH MRI agent. We further showed that the sensitivity of iopamidol pH imaging peaked at an intermediate RF irradiation level, and iopamidol CEST MRI is suitable for measuring pH between 6 and 7.5 with an accuracy of 0.1 pH unit despite that  $T_1$  and  $T_2$  measurements varied substantially with pH and concentration. Our study remains promising to help optimize and translate iopamidol pH imaging to the clinic.

TABLE

$k_{\text{SW}} \text{ (s}^{-1}\text{)}$ pH	$k_{\text{SW}} \text{ (5.5 ppm)}$	$k_{\text{SW}} \text{ (4.3 ppm)}$	$k_{\text{SW}} \text{ (1.8 ppm)}$	$k_{\text{SW}} \text{ (0.8 ppm)}$
5.5	$47 \pm 12 \text{ s}^{-1}$	$7 \pm 4 \text{ s}^{-1}$	$388 \pm 157 \text{ s}^{-1}$	$2070 \pm 331 \text{ s}^{-1}$
6	$87 \pm 34 \text{ s}^{-1}$	$17 \pm 6 \text{ s}^{-1}$	$242 \pm 188 \text{ s}^{-1}$	$1759 \pm 519 \text{ s}^{-1}$
6.5	$265 \pm 65 \text{ s}^{-1}$	$67 \pm 15 \text{ s}^{-1}$	$416 \pm 166 \text{ s}^{-1}$	$1856 \pm 1567 \text{ s}^{-1}$
7	$1074 \pm 298 \text{ s}^{-1}$	$190 \pm 25 \text{ s}^{-1}$	$1104 \pm 337 \text{ s}^{-1}$	$1715 \pm 483 \text{ s}^{-1}$
7.5	$2896 \pm 285 \text{ s}^{-1}$	$868 \pm 260 \text{ s}^{-1}$	$9262 \pm 6138 \text{ s}^{-1}$	$5117 \pm 4485 \text{ s}^{-1}$

Table 1, Numerically determined pH-dependent exchange rates for labile protons at 5.5 (2-hydroxypropanamido group), 4.3 (amide group), 1.8 (secondary hydroxyl group) and 0.8 (primary hydroxyl groups) ppm. Data are shown in mean  $\pm$  standard deviation. The relative labile proton ratio for 5.5, 4.3, 1.8 and 0.8 ppm was fixed to be 1:2:1:4, with labile proton ratio at 5.5 ppm determined to be  $1:3449 \pm 747$ .

## FIGURES

Fig. 1

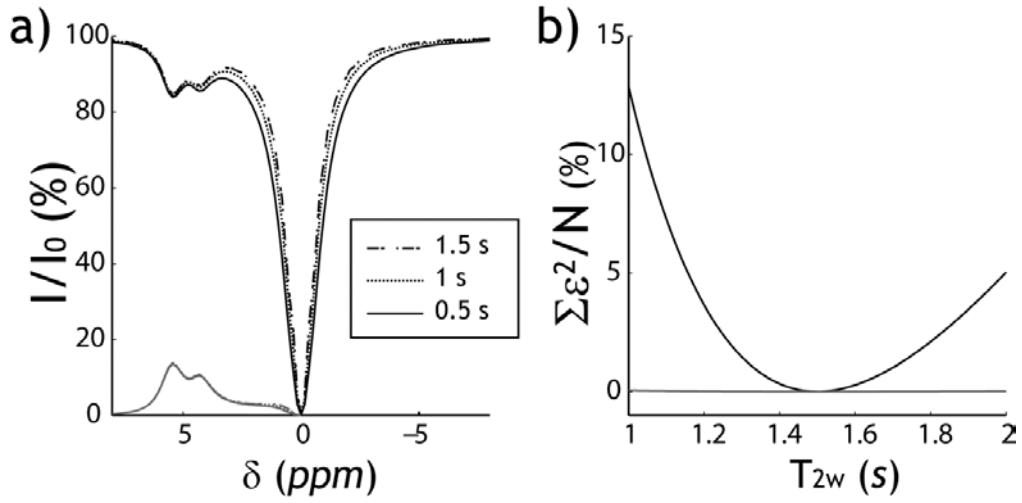


Fig. 1, a) Simulated CEST Z-spectra and asymmetry-plots for three representative bulk water  $T_{2w}$  of 0.5, 1 and 1.5 s. ( $B_1 = 2.5 \mu\text{T}$ ). b) Two plots of sum of squares analysis of the difference in simulated CEST Z-spectra (black) and asymmetry plots (gray) as a function of  $T_{2w}$  from those obtained assuming the median

$$T_{2w} \text{ (i.e., } \sum_{i=1}^N \left( I_{i,T_{2w}} - I_{i,\overline{T_{2w}}} \right)^2 / N \text{ )}.$$

Fig. 2

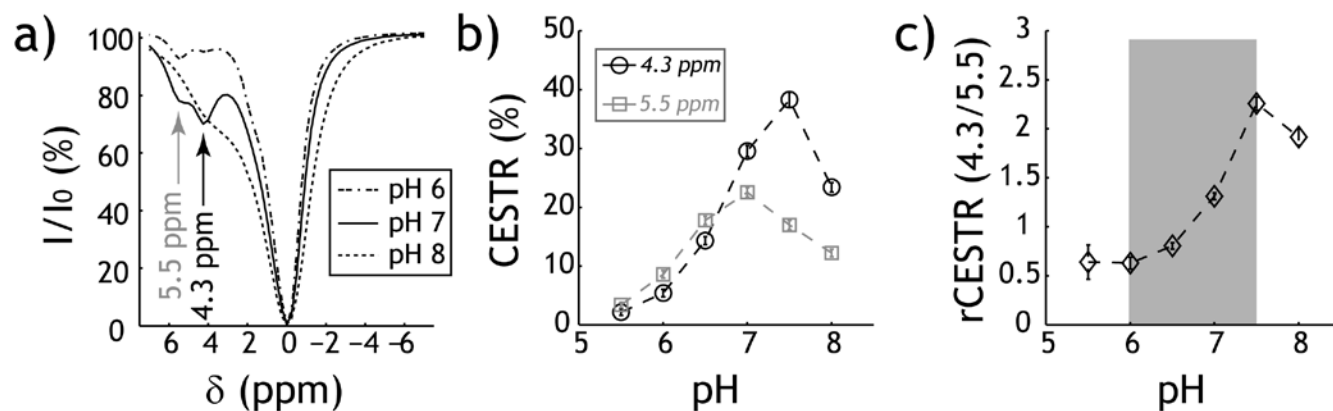


Fig. 2, Iopamidol ratiometric pH MRI. a) Z-spectra for representative pH of 6, 7 and 8 ( $B_1 = 2.5 \mu T$ ,  $TS = 5s$ ) at room temperature. b) CEST ratio (CESTR) calculated from the asymmetry analysis as a function of pH. CESTR at 4.3 ppm peaks at pH 7.5 while CESTR of 5.5 ppm peaks at pH 7. c) Ratiometric CEST analysis is sensitive to pH ranging from 6 to 7.5.

Fig. 3

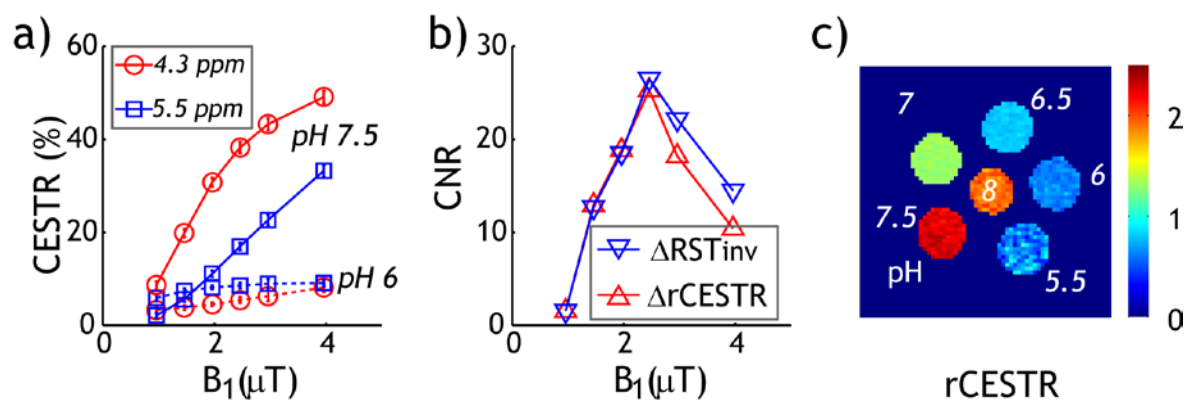


Fig. 3, B<sub>1</sub>-dependence of iopamidol ratiometric pH MRI. a) CESTR at 4.3 and 5.5 ppm increases with B<sub>1</sub> irradiation level for representative pH of 6 and 7.5. b) CNR in ratiometric pH MRI between pH of 6 and 7.5 peaks under an intermediate optimal B<sub>1</sub> level of 2.5 μT. c) pH-weighted rCESTR map (B<sub>1</sub> = 2.5 μT).



Fig. 4

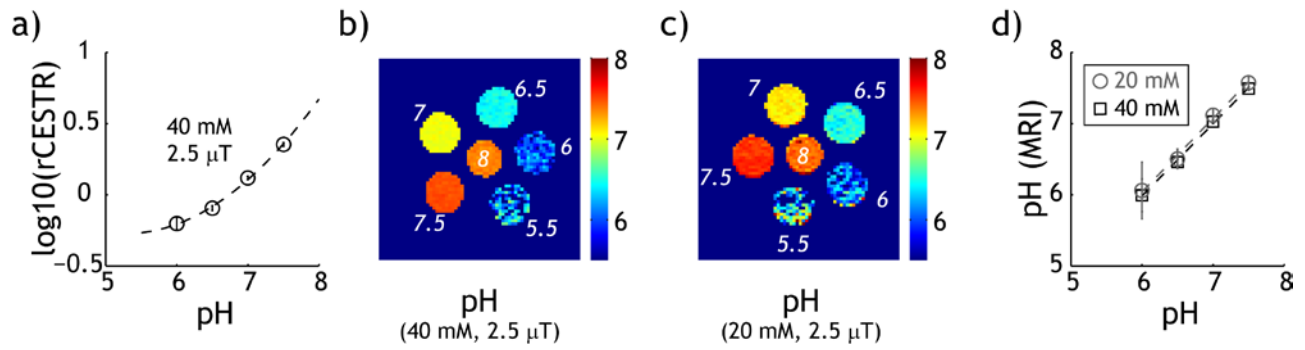


Fig. 4, Evaluation of the accuracy of iopamidol pH imaging. a) Logarithmic rCESTR as a function of pH for 40 mM iopamidol. b) pH map determined from pH-weighted rCESTR map for 40 mM iopamidol. c) pH map determined from pH-weighted rCESTR map for 20 mM iopamidol. d) pH determined from iopamidol pH MRI vs. titrated pH for 20 mM (circles) and 40 mM (squares) iopamidol phantoms.

Fig. 5

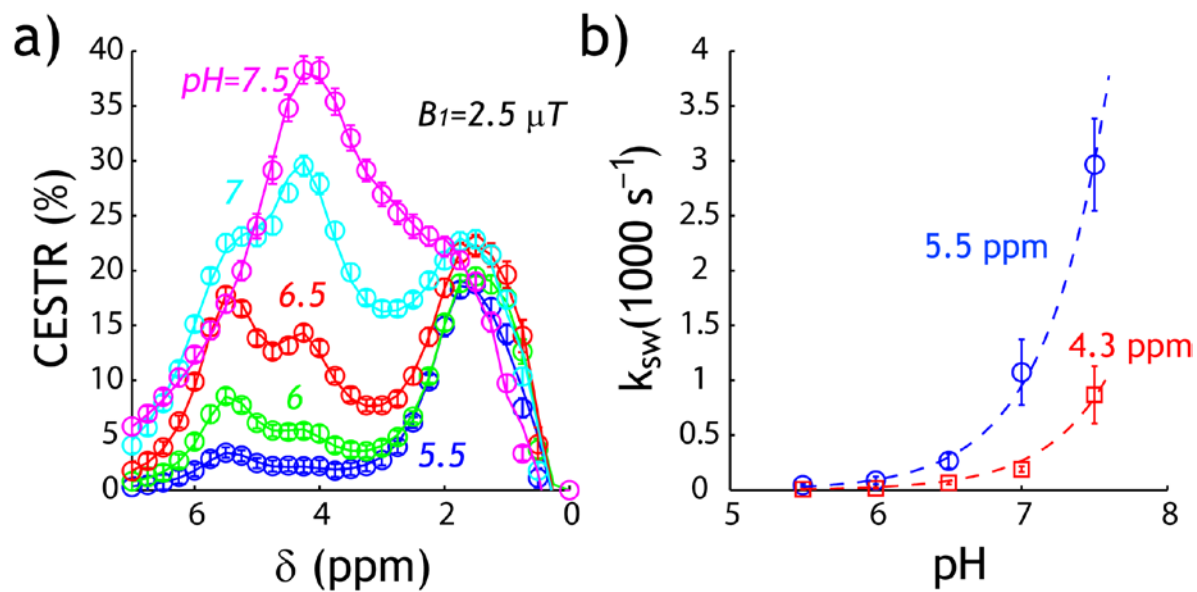


Fig. 5, Numerical solution of iopamidol pH-dependent chemical exchange properties. a) Numerical fitting of asymmetry plots ( $B_1 = 2.5 \mu T$ ). b) Numerically determined pH-dependent chemical exchange for labile protons at 4.3 and 5.5 ppm.

## REFERENCES

- Adam W R, Koretsky A P and Weiner M W 1986  $^{31}\text{P}$ -NMR in vivo measurement of renal intracellular pH: effects of acidosis and  $\text{K}^+$  depletion in rats *Am J Physiol Cell Physiol* **251** F904-10
- Aime S, Barge A, Delli Castelli D, Fedeli F, Mortillaro A, Nielsen F U and Terreno E 2002 Paramagnetic Lanthanide(III) complexes as pH-sensitive chemical exchange saturation transfer (CEST) contrast agents for MRI applications *Magn. Reson. Med.* **47** 639-48
- Aime S, Calabi L, Biondi L, Miranda M D, Ghelli S, Paleari L, Rebaudengo C and Terreno E 2005 Iopamidol: Exploring the potential use of a well-established x-ray contrast agent for MRI *Magn Reson Med.* **53** 830-4
- Ali M M, Liu G, Shah T, Flask C A and Pagel M D 2009 Using Two Chemical Exchange Saturation Transfer Magnetic Resonance Imaging Contrast Agents for Molecular Imaging Studies *Acc. Chem. Res.* **42** 915-24
- Allerhand A, Gutowsky H, Jonas J and Meinzer R 1966 Nuclear magnetic resonance methods for determining chemical-exchange rates *J Am Chem Soc* **88** 3185-93
- Castelli D D, Terreno E, Longo D and Aime S 2013 Nanoparticle-based chemical exchange saturation transfer (CEST) agents *NMR in Biomedicine* **26** 839-49
- Chan K W Y, Liu G, Song X, Kim H, Yu T, Arifin D R, Gilad A A, Hanes J, Walczak P, van Zijl P C M, Bulte J W M and McMahon M T 2013 MRI-detectable pH nanosensors incorporated into hydrogels for in vivo sensing of transplanted-cell viability *Nat Mater* **12** 268-75
- Chen L Q, Howison C M, Jeffery J J, Robey I F, Kuo P H and Pagel M D 2013 Evaluations of extracellular pH within in vivo tumors using acidoCEST MRI *Magn Reson Med* in press
- Dagher A P, Aletras A, Choyke P and Balaban R S 2000 Imaging of urea using chemical exchange-dependent saturation transfer at 1.5T *J. Magn. Reson. Imaging* **12** 745-8
- Dula A N, Asche E M, Landman B A, Welch E B, Pawate S, Sriram S, Gore J C and Smith S A 2012 Development of chemical exchange saturation transfer at 7T *Magn Reson Med* **66** 831-8
- Frullano L, Catana C, Benner T, Sherry A D and Caravan P 2010 Bimodal MR-PET Agent for Quantitative pH Imaging *Angew Chem Int Ed Engl* **49** 2382-4
- Henkelman R M, Stanisz G J, Kim J K and Bronskill M J 1994 Anisotropy of NMR properties of tissues *Magn Reson Med* **32** 592-601

- Hingorani D V, Randtke E A and Pagel M D 2013 A CatalyCEST MRI Contrast Agent That Detects the Enzyme-Catalyzed Creation of a Covalent Bond *J Am Chem Soc.* **135** 6396-8
- Jin T, Wang P, Zong X and Kim S-G 2012 Magnetic resonance imaging of the Amine Proton EXchange (APEX) dependent contrast *NeuroImage* **16** 1218-27
- Jokivarsi K T, Gröhn H I, Gröhn O H and Kauppinen R A 2007 Proton transfer ratio, lactate, and intracellular pH in acute cerebral ischemia *Magn Reson Med* **57** 647-53
- Jones C K, Huang A, Xu J, Edden R A E, Schäfer M, Hua J, Oskolkov N, Zaccarelli D, Zhou J, McMahon M T, Pillai J J and van Zijl P C M 2013 Nuclear Overhauser enhancement (NOE) imaging in the human brain at 7 T *NeuroImage* **77** 114-24
- Kogan F, Haris M, Singh A, Cai K, Debrosse C, Nanga R P R, Hariharan H and Reddy R 2014 Method for high-resolution imaging of creatine in vivo using chemical exchange saturation transfer *Magn Reson Med* **71** 164-72
- Li A X, Hudson R H E, Barrett J W, Johns C K, Pasternak S H and Bartha R 2008 Four-pool modeling of proton exchange processes in biological systems in the presence of MRI-paramagnetic chemical exchange saturation transfer (PARACEST) agents *Magn Reson Med* **60** 1197-206
- Liu G, Li Y, Sheth V R and Pagel M D 2012 Imaging In Vivo Extracellular pH with a Single Paramagnetic Chemical Exchange Saturation Transfer Magnetic Resonance Imaging Contrast Agent *Molecular Imaging* **11** 47-57
- Longo D L, Busato A, Lanzardo S, Antico F and Aime S 2012 Imaging the pH evolution of an acute kidney injury model by means of iopamidol, a MRI-CEST pH-responsive contrast agent *Magn Reson Med* **70** 859-64
- Longo D L, Dastrù W, Digilio G, Keupp J, Langereis S, Lanzardo S, Prestigio S, Steinbach O, Terreno E, Uggeri F and Aime S 2011 Iopamidol as a responsive MRI-chemical exchange saturation transfer contrast agent for pH mapping of kidneys: In vivo studies in mice at 7 T *Magn Reson Med* **65** 202-11
- McMahon M, Gilad A, Zhou J, Sun P Z, Bulte J and van Zijl P C 2006 Quantifying exchange rates in chemical exchange saturation transfer agents using the saturation time and saturation power dependencies of the magnetization transfer effect on the magnetic resonance imaging signal (QUEST and QUESP): Ph calibration for poly-L-lysine and a starburst dendrimer *Magn Reson Med.* **55** 836-47
- Murase K and Tanki N 2011 Numerical solutions to the time-dependent Bloch equations revisited *Magn Reson Imaging* **29** 126-31

- Olatunde A O, Dorazio S J, Sperryak J A and Morrow J R 2012 The NiCEST Approach: Nickel(II) ParaCEST MRI Contrast Agents *J . Am. Chem. Soc.* **134** 18503-5
- Scheidegger R, Vinogradov E and Alsop D C 2011 Amide proton transfer imaging with improved robustness to magnetic field inhomogeneity and magnetization transfer asymmetry using saturation with frequency alternating RF irradiation *Magn Reson Med* **66** 1275-85
- Schmitt B, Zaiß M, Zhou J and Bachert P 2011 Optimization of pulse train presaturation for CEST imaging in clinical scanners *Magn Reson Med* **65** 1620-9
- Sheth V R, Li Y, Chen L Q, Howison C M, Flask C A and Pagel M D 2012 Measuring in vivo tumor pHe with CEST-FISP MRI *Magn Reson Med* **67** 760-8
- Sun P Z 2010a Simplified and scalable numerical solution for describing multi-pool chemical exchange saturation transfer (CEST) MRI contrast *J. Magn. Reson.* **205** 235-41
- Sun P Z 2010b Simultaneous determination of labile proton concentration and exchange rate utilizing optimal RF power: radio frequency power (RFP) dependence of chemical exchange saturation transfer (CEST) MRI. *J. Magn. Reson.* **202** 155-61
- Sun P Z 2012 Simplified quantification of labile proton concentration-weighted chemical exchange rate (kws) with RF saturation time dependent ratiometric analysis (QUESTRA): Normalization of relaxation and RF irradiation spillover effects for improved quantitative chemical exchange saturation transfer (CEST) MRI *Magn Reson Med* **67** 936-42
- Sun P Z, Benner T, Kumar A and Sorensen A G 2008 Investigation of optimizing and translating pH-sensitive pulsed-chemical exchange saturation transfer (CEST) imaging to a 3T clinical scanner *Magn Reson Med* **60** 834-41
- Sun P Z, Cheung J S, Wang E F and Lo E H 2011a Association between pH-weighted endogenous amide proton chemical exchange saturation transfer MRI and tissue lactic acidosis during acute ischemic stroke *J. Cereb. Blood Flow Metab.* **31** 1743-50
- Sun P Z, Lu J, Wu Y, Xiao G and Wu R 2013a Evaluation of the dependence of CEST-EPI measurement on repetition time, RF irradiation duty cycle and imaging flip angle for enhanced pH sensitivity *Phys Med Biol.* **58** N229-N40

- Sun P Z and Sorensen A G 2008 Imaging pH using the chemical exchange saturation transfer (CEST) MRI: correction of concomitant RF irradiation effects to quantify CEST MRI for chemical exchange rate and pH *Magn Reson Med* **60** 390-7
- Sun P Z, van Zijl P C M and Zhou J 2005 Optimization of the irradiation power in chemical exchange dependent saturation transfer experiments *J Magn Reson* **175** 193-200
- Sun P Z, Wang E F and Cheung J S 2012 Imaging acute ischemic tissue acidosis with pH-sensitive endogenous amide proton transfer (APT) MRI - Correction of tissue relaxation and concomitant RF irradiation effects toward mapping quantitative cerebral tissue pH. *Neuroimage* **60** 1-6
- Sun P Z, Wang E F, Cheung J S, Zhang X A, Benner T and Sorensen A G 2011b Simulation and optimization of pulsed radio frequency (RF) irradiation scheme for chemical exchange saturation transfer (CEST) MRI - demonstration of pH-weighted pulsed-amide proton CEST MRI in an animal model of acute cerebral ischemia. *Magn Reson Med* **66** 1042-8
- Sun P Z, Wang Y, Dai Z, Xiao G and Wu R 2014a Quantitative chemical exchange saturation transfer (qCEST) MRI - RF spillover effect-corrected omega plot for simultaneous determination of labile proton fraction ratio and exchange rate *Contrast Media Mol Imaging* **9** 268-75
- Sun P Z, Wang Y and Lu J 2014b Sensitivity-enhanced chemical exchange saturation transfer (CEST) MRI with least squares optimization of Carr Purcell Meiboom Gill multi-echo echo planar imaging *Contrast Media & Molecular Imaging* **9** 177-81
- Sun P Z, Wang Y, Xiao G and Wu R 2013b Simultaneous experimental determination of labile proton fraction ratio and exchange rate with irradiation radio frequency power-dependent quantitative CEST MRI analysis *Contrast Media Mol Imaging* **8** 246-51
- Sun P Z, Zhou J, Huang J and van Zijl P 2007a Simplified quantitative description of amide proton transfer (APT) imaging during acute ischemia *Magn Reson Med* **57** 405-10
- Sun P Z, Zhou J, Sun W, Huang J and van Zijl P C 2007b Detection of the ischemic penumbra using pH-weighted MRI *J Cereb Blood Flow Metab* **27** 1129-36
- Terreno E, Dastrù W, Delli Castelli D, Gianolio E, Geninatti Cich S, Longo D and Aime S 2010 Advances in metal-based probes for MR molecular imaging applications *Curr Med Chem* **17** 3684-70
- van Zijl P C M and Yadav N N 2011 Chemical exchange saturation transfer (CEST): What is in a name and what isn't? *Magn Reson Med* **65** 927-48

- Vinogradov E, Sherry A D and Lenkinski R E 2013 CEST: From basic principles to applications, challenges and opportunities *J Magn Reson* **229** 155-72
- Ward K M, Aletras A H and Balaban R S 2000 A new class of contrast agents for MRI based on proton chemical exchange dependent saturation transfer (CEST) *J. Magn. Reson.* **143** 79-87
- Ward K M and Balaban R S 2000 Determination of pH using water protons and chemical exchange dependent saturation transfer (CEST) *Magnetic Resonance in Medicine* **44** 799-802
- Woessner D E, Zhang S, Merritt M E and Sherry A D 2005 Numerical solution of the Bloch equations provides insights into the optimum design of PARACEST agents for MRI *Magn Reson Med.* **53** 790-9
- Woods M, Woessner D E and Sherry A D 2006 Paramagnetic lanthanide complexes as PARACEST agents for medical imaging *Chem Soc Rev* **35** 500-11
- Wu R, Liu C, Liu P and Sun P Z 2012 Improved measurement of labile proton concentration-weighted chemical exchange rate (k<sub>ex</sub>) with experimental factor-compensated and T<sub>1</sub>-normalized quantitative chemical exchange saturation transfer (CEST) MRI *Contrast Media Mol Imaging* **7** 384-9
- Zaiss M and Bachert P 2013 Exchange-dependent relaxation in the rotating frame for slow and intermediate exchange - modeling off-resonant spin-lock and chemical exchange saturation transfer *NMR in Biomedicine* **26** 507-18
- Zhang S, Malloy C R and Sherry A D 2005 MRI Thermometry Based on PARACEST Agents *J. Am. Chem. Soc.* **127** 17572-3
- Zhou J, Wilson D A, Sun P Z, Klaus J A and van Zijl P C M 2004 Quantitative description of proton exchange processes between water and endogenous and exogenous agents for WEX, CEST, and APT experiments *Magn Reson Med* **51** 945-52
- Zhu H, Jones C K, van Zijl P C M, Barker P B and Zhou J 2010 Fast 3D chemical exchange saturation transfer (CEST) imaging of the human brain *Magn Reson Med* **64** 638-44
- Zu Z, Janve V A, Li K, Does M D, Gore J C and Gochberg D F 2012 Multi-angle ratiometric approach to measure chemical exchange in amide proton transfer imaging *Magn Reson Med* **68** 711-9
- Zu Z, Li K, Janve V A, Does M D and Gochberg D F 2011 Optimizing pulsed-chemical exchange saturation transfer imaging sequences *Magn Reson Med* **66** 1100-8